Rotational Motions in Atactic Poly(acrylonitrile) Studied by One- and Two-Dimensional ^{15}N Solid-State NMR and Dielectric Measurements

Hironori Kaji,*,†,‡,§ Nobuhiro Miura,† and Klaus Schmidt-Rohr†,⊥

Department of Polymer Science and Engineering, University of Massachusetts, Amherst, Massachusetts 01003; Institute for Chemical Research, Kyoto University, Uji, Kyoto 611-0011, Japan; PRESTO, Japan Science and Technology Corporation, Uji, Kyoto 611-0011, Japan; and Department of Chemistry and Ames Laboratory, Iowa State University, Ames, Iowa 50011

Received February 3, 2003; Revised Manuscript Received June 5, 2003

ABSTRACT: The dynamics of atactic poly(acrylonitrile) (aPAN) have been investigated by variable-temperature ^{15}N chemical shift anisotropy (CSA), two-dimensional (2D) ^{15}N CSA exchange, and 2D ^{15}N pure-exchange NMR experiments on an aPAN sample with 100% ^{15}N-labeled nitrile side groups and by dielectric measurements. In contrast to the dynamics below 110 °C, where only small-angle motions are observed with an activation energy $E_a = 68$ kJ mol^{-1}, it is found that large-amplitude motions with $E_a = 180$ kJ mol^{-1} set in above 110 °C. From the detailed analysis of the NMR spectra, it is found that aPAN undergoes restricted uniaxial rotational diffusion motion around the chain axis above 110 °C. The 2D spectra prove that there is a distribution of amplitudes of these restricted motions. The standard deviation of the amplitude distribution increases from 30° to 100° in the temperature range 120−140 °C. At the highest temperature, there is strong evidence of dynamic averaging within the distribution of angles between the C≡N bond and the fiber axis. The experimental findings indicate that the motion occurs in the disordered pseudohexagonal lattice and thus favor a single-phase model for aPAN. An alternative explanation by crankshaft motion can be ruled out mainly by the small gauche content of 10%, which is confirmed by variable-temperature ^{13}C CP/MAS experiments. The solid-state NMR results are in excellent agreement with those in dielectric relaxation experiments, where a relaxation peak of growing amplitude and frequency position is observed.

1. Introduction

Atactic poly(acrylonitrile), aPAN, a polymer with lateral long-range order, is widely used as a material for textiles and precursors of carbon fibers. However, the chain conformation is disordered, and the details of the disordered conformation, the chain dynamics, and the phase structure have remained controversial. In our preceding papers,[1−3] the torsion angle distributions in aPAN have been measured quantitatively and selectively for meso and racemo dyads by various newly developed two-dimensional solid-state NMR methods. The backbone conformation in aPAN was determined as 90% trans (±5%).[4] The successive average torsion angles and their distributions in racemo trans−trans dyads have been determined to be 180 ± 5° with standard deviations of $\sigma = 10 \pm 5°$. In contrast, the successive torsion angles in meso trans−trans dyads were found to deviate from 180° trans on average by 10°−20° and to be broadly distributed with $\sigma = 20 \pm 5°$. In contrast, the phase structure and the dynamics are still uncertain. Some researchers observed only one relaxation at 100−110 °C. Others reported two relaxations at 70−110 and 120−160 °C. Sometimes, three relaxations were observed, as recently reviewed by Bashir.[5] On the basis of the observations, one-, two-, and three-phase models have been proposed by various authors. The assignments of these relaxations are still controversial together with the phase structure: in studies that reported two relaxations in aPAN, the transitions at lower temperature and higher temperature have been assigned to motions in crystalline and amorphous regions, respectively. The assignment for the lower temperature relaxation is based on the observation of a corresponding transition in the X-ray *d*-spacing for a crystalline diffraction peak.[6,7] If this is correct and if aPAN is semicrystalline, this leads to an unusual result; the relaxation temperature in the crystalline regions would be lower than that in the amorphous regions.[5,8] However, recent WAXD,[9,10] ^2H NMR,[11] and two-dimensional NMR[1−3] experiments favor a single-phase model.[12] The details, such as the motional amplitude, geometry, rate, and activation energy, of the chain dynamics underlying the relaxations are important aspects that have not been elucidated yet.

In this article, we characterize the dynamics in unoriented aPAN between −60 and 140 °C. For this purpose, one-dimensional (1D) ^{15}N chemical shift anisotropy (CSA) measurements as well as two-dimensional (2D) ^{15}N CSA exchange and pure-exchange (PUREX) experiments[14] are carried out for a 100% ^{15}N-labeled aPAN (^{15}N-aPAN) sample. ^{15}N nuclei in aPAN are good probes for characterizing the dynamics of aPAN, since ^{15}N in a nitrile group has an axially symmetric ^{15}N CSA tensor. Its unique axis points along the C≡N bond; thus, reorientations of this bond can be measured directly. With an angle θ between the C≡^{15}N direction and the external magnetic field B_0 at a given time, the ^{15}N anisotropic chemical shift frequency is

$$\omega_a(\theta) = \frac{\delta}{2}(3\cos^2\theta - 1) \qquad (1)$$

The −C≡N directions corresponding to the chemical shifts of $\sigma_{\parallel} = \sigma_{iso} + \delta$ and $\sigma_{\perp} = \sigma_{iso} - \delta/2$ are parallel and

† University of Massachusetts.
‡ Kyoto University.
§ Japan Science and Technology Corporation.
⊥ Iowa State University.
* To whom correspondence should be addressed. E-mail: kaji@scl.kyoto-u.ac.jp.

10.1021/ma0341420 CCC: $25.00
Published on Web 07/12/2003

perpendicular, respectively, to the static magnetic field, B_0. The ^{15}N CSA spectrum is less complicated compared to ^2H and ^{13}C powder patterns: two transitions are inevitably overlapped for ^2H spectra of a deuterated aPAN sample, and the ^{13}C CSA spectra of a $^{13}C{\equiv}N$-carbon labeled aPAN sample consist of three similar powder patterns due to the directly bonded $^{13}C{\equiv}^{14}N$ dipolar coupling.[2]

We also carried out two additional NMR experiments, which are indispensable for the elucidation of the motional geometry in aPAN. To investigate possible changes in the trans/gauche ratio over the 20−140 °C temperature range, $^{13}CH_2$ isotropic chemical shifts were measured. Separation of the overlapping CH_2 and CH resonances was achieved by subtracting the ^{13}C CP/MAS NMR spectrum of an unlabeled aPAN powder sample from that of a 15% $^{13}CH_2$-carbon labeled aPAN ($^{13}CH_2$-aPAN) powder sample. The $-C{\equiv}N$ orientations relative to the chain axis are determined from ^{13}C static CP NMR spectra of uniaxially oriented unlabeled aPAN fibers.

Dielectric experiments give useful dynamics information. However, the data reported on aPAN by several authors are not consistent,[15−19] which may be due to differences in sample synthesis, processing, etc. Therefore, we also carried out dielectric measurements by using the same PAN material and similar processing as used for the NMR experiments. The dynamics characterized by the above-mentioned NMR techniques can explain the results of the dielectric measurements.

2. Experimental Section

2.1. Samples. A powdered 100% ^{15}N-labeled aPAN (^{15}N-aPAN) sample was polymerized from acrylonitrile-^{15}N. The details of the polymerization procedure, the polymer processing, and the characterization of the polymer were described in our preceding paper.[1] The viscosity average molecular weight was 1.2×10^5, and the triad tacticity measured by solution ^{13}C NMR was *mm*:*mr*:*rr* = 29:50:21. The wide-angle X-ray diffraction (WAXD) pattern showed pseudohexagonal chain packing, which is the most commonly reported polymorph.[6,9,10,20,21] The sample was pressed into the shape of a cylindrical block for ^{15}N solid-state NMR experiments. A $^{13}CH_2$-aPAN and an unlabeled aPAN sample, used for ^{13}C CP/MAS NMR experiments, were the same materials analyzed in our previous paper.[1] The unlabeled aPAN sample was also used for the dielectric measurements; the sample processing is also the same except that the sample was hot-pressed to make thin films with 0.2−0.5 mm thickness. Uniaxially oriented unlabeled aPAN fibers were produced by wet spinning from an aqueous sodium thiocyanate (NaSCN) solution and subsequent stretching in the dry state. The total draw ratio was 15. The viscosity-average molecular weight was 2.5×10^5, and the triad tacticity measured by solution ^{13}C NMR was *mm*:*mr*:*rr* = 28:51:21.

2.2. NMR Measurements. The solid-state NMR experiments without MAS were performed on a Bruker DSX-300 spectrometer in a static magnetic field of 7 T. The chemical shifts are referenced to the isotropic chemical shift for all the ^{15}N NMR experiments. For ^{13}C NMR experiments, the chemical shifts are referenced to tetramethylsilane (Me_4Si) via secondary standards. Since the phase structure of aPAN is not well understood yet,[22] we measured all the components in aPAN, without using any relaxation-time filters for the selection of certain morphological components. The phase structure of aPAN is discussed in ref 1 and further below in this paper. The temperatures for static experiments were calibrated using Hg thermometers.

2.2.1. ^{15}N CSA Measurements. 1D ^{15}N CSA and 2D exchange measurements were carried out with a 5 mm diameter coil of a stationary probe. The ^1H 90° and ^{15}N 180° pulse lengths were 3.4−3.8 and 9.6−11.6 μs, respectively. A cross-polarization time of 2−5 ms, a recycle delay of 4−5 s, an acquisition time of 3.71 ms, a dwell time of 7.15 μs, and ^1H decoupling fields $\gamma B_1/2\pi$ of ca. 66.5 kHz were used. The delay for the Hahn echo before detection was $2\tau = 100$ μs. All the pulses were applied at a frequency near the center of the powder spectrum. For each 1D spectrum, 1024−8192 scans were accumulated, and the total acquisition time was 1.1−11.4 h, depending on the temperature of measurement.

For the 2D ^{15}N CSA exchange experiments, 84−344 slices with increments of 14.3 μs were acquired in the t_1 dimension, with 32−320 scans per each t_1 slice. Both cosine and sine data sets were measured on-resonance in ω_1 and ω_2, to give hypercomplex data sets. The total acquisition time per spectrum was 9.1−62.6 h depending on the measurement temperature and mixing time used.

2.2.2. 2D ^{15}N PUREX Measurements. A 2D ^{15}N PUREX experiment was carried out at 20 °C with a mixing time of 1 s. The delay τ for creating cosine or sine modulation in eq 2 (see below) was 0.5 ms. A cross-polarization time of 2 ms and a recycle delay of 2 s were used. The ^{15}N frequency was switched 15 kHz off-resonance during the t_1 evolution time, and cosine data sets were measured off-resonance in ω_1 and processed to yield purely absorptive, nonquadrature spectra.[2] The free induction decays were acquired with a frequency near the center of the powder spectrum. In the t_1 dimension, 64 slices with increments of 14.3 μs were acquired, with 64 scans per each t_1 slice. All the other parameters were the same as for the 2D ^{15}N CSA exchange experiments. The total acquisition time was 6.8 h.

The goal of the PUREX experiment is the removal of the dominant but trivial diagonal ridge from the 2D exchange spectrum, together with all its accompanying artifacts. This enables in particular the markedly improved detection of the exchange signals from small-angle motions, which appear near the diagonal. The suppression of the diagonal is achieved by incorporating two extra delays before and after the mixing time of a standard 2D exchange pulse sequence to give $\cos(\Omega_1\tau)\cos(\Omega_2\tau)S$ or $\sin(\Omega_1\tau)\sin(\Omega_2\tau)S$, depending on the pulse phases used. Here, Ω_1 and Ω_2 are the NMR frequencies before and after the mixing time, respectively, τ is the delay incorporated in the pulse sequence, and S is the standard 2D exchange signal. The combination of three data sets (unmodulated, cosine-modulated, and sine-modulated) gives a sine-square-modulated 2D signal:

$$S - \cos(\Omega_1\tau)\cos(\Omega_2\tau)S - \sin(\Omega_1\tau)\sin(\Omega_2\tau)S = S - S\cos((\Omega_1 - \Omega_2)\tau) = 2S\sin^2((\Omega_1 - \Omega_2)\tau/2) \quad (2)$$

Suppression of the diagonal ridge is thus found to be realized because the standard 2D spectrum is modulated by $\sin^2((\Omega_1 - \Omega_2)\tau/2)$, which does not give any signals at the diagonal of $\Omega_1 = \Omega_2$. Further details of 2D PUREX experiments are described in the original paper.[14]

2.2.3. 1D ^{13}C Static CP Experiments for Uniaxially Oriented aPAN Fibers. 1D ^{13}C static CP experiments of uniaxially oriented aPAN fibers were carried out with a 7.5 mm diameter flat coil of a stationary probe at 20 °C. The ^1H and ^{13}C 90° pulse lengths were 5.3 μs. A cross-polarization time of 2.0 ms, a recycle delay of 10 s, an acquisition time of 3.12 ms, a dwell time of 6.0 μs, and a ^1H decoupling field strength $\gamma B_1/2\pi = 37.5$ kHz were used. The delay for the Hahn echo before detection was $2\tau = 54$ μs. For the sample alignments with the fiber axes parallel to and perpendicular to B_0, 4000 and 8000 scans were accumulated, respectively.

2.2.4. 1D ^{13}C CP/MAS Measurements. 1D ^{13}C CP/MAS experiments were carried out in a 7.5 mm CP/MAS probe using a Chemagnetics CMX-400 spectrometer. The ^1H and ^{13}C 90° pulse lengths were 4.0 μs. The cross-polarization time was 1.0−0.2 ms depending on the temperature. A recycle delay of 4 s, an acquisition time of 6.4 ms, a dwell time of 12.5 μs, and a ^1H decoupling field strength of $\gamma B_1/2\pi = 50$ kHz were used. For each spectrum, 256−1024 scans were accumulated. To observe the CH_2 resonance line selectively, the overlapping

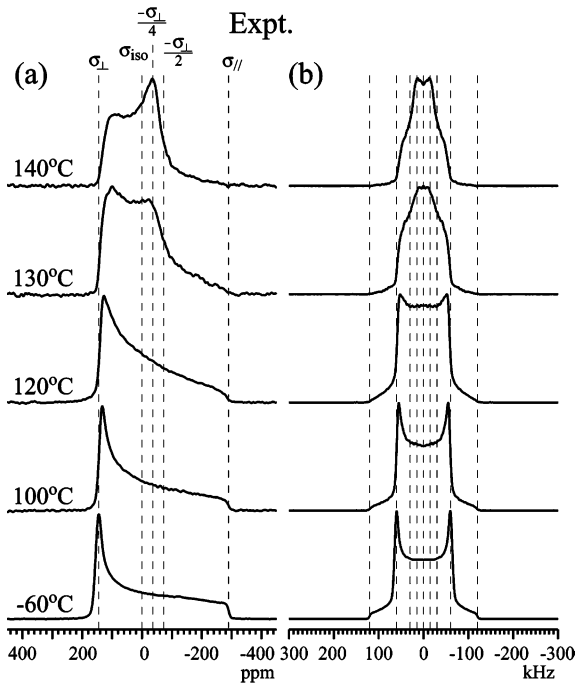

Figure 1. (a) Experimental one-dimensional (1D) ^{15}N CSA spectra of ^{15}N-aPAN from −60 to 140 °C. The chemical shift is referenced to the isotropic chemical shift of ^{15}N-aPAN, σ_{iso}. A Hahn echo with a total delay time, 2τ, of 0.1 ms is used before detection. (b) Symmetrized experimental 1D ^{15}N CSA spectra of ^{15}N-aPAN from −60 to 140 °C. The chemical shifts, in kHz, have been multiplied by 13.6 to give the corresponding ^{2}H quadrupolar frequencies. Finite-pulse-width corrections have been applied to the symmetrized spectra to permit direct comparison with the ^{2}H spectra in ref 11.

CH resonance line was removed by subtracting the spectrum of an unlabeled aPAN sample from that of the $^{13}CH_2$-aPAN sample, using the natural abundance $^{13}C{\equiv}N$ signals to determine the exact scaling of the subtracted spectra at 22, 60, and 100 °C. This procedure could not be applied for the spectrum at 140 °C, where the $^{13}C{\equiv}N$ signal is too broad to be observed reliably. However, the scaling factor was reasonably estimated from the factors at 22−100 °C. The temperatures for these experiments were the calibrated temperatures by the ethylene glycol method[23,24] and ^{207}Pb NMR measurements.[25,26]

2.3. Dielectric Measurements. Dielectric measurements were carried out using a broadband dielectric spectrometer (Novocontrol GmbH). This system includes a Solatron-Schlumberger gain/phase analyzer SI1260 and high impedance buffer amplifier (Chelsea Dielectric Interface). The experiments were performed at fixed temperatures, and the frequency dependence of the complex dielectric constant was measured over a frequency range of 10^{-1}−10^{6} Hz.

3. Results

3.1. 1D and 2D ^{15}N NMR: Small-Angle Motion below 110 °C. Figure 1a shows a series of one-dimensional (1D) ^{15}N CSA spectra of a ^{15}N-aPAN sample, measured as a function of temperature. Below 110 °C, the change of CSA line shapes is very small. To display the small change more clearly, the temperature dependence of the spectrum width, $\sigma_\perp - \sigma_{//}$, which corresponds to $-{}^3/_2\delta$ in eq 1, and the chemical shift values of the peak at $\sigma_\perp$ are plotted in Figure 2 in kilohertz. This figure shows the narrowing of CSA widths with increasing temperature, indicating that the $-C{\equiv}N$ side group, and therefore the main chain, undergoes small-angle motions below 110 °C.

In Figure 3, experimental 2D ^{15}N CSA exchange spectra of a ^{15}N-aPAN sample are shown. Near-diagonal

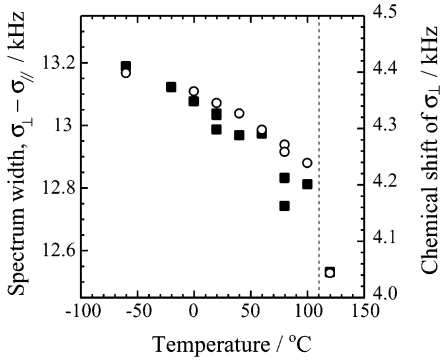

Figure 2. Temperature dependences of the full width of the CSA spectrum, $\sigma_\perp - \sigma_{//}$, and of the chemical shift principal value, $\sigma_\perp$, shown by filled squares and open circles, respectively. The chemical shift values of $\sigma_{//}$ are not clear for the spectra at 130 and 140 °C. The chemical shift values of $\sigma_\perp$ are ca. 3.1 and 2.7 kHz at 130 and 140 °C, respectively, which is far below the range shown in this figure.

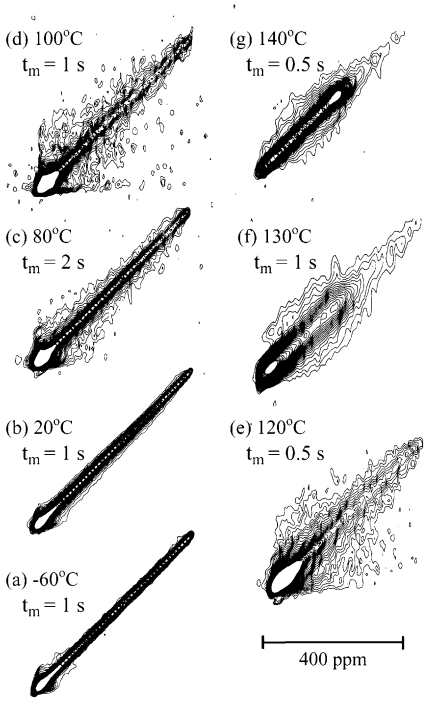

Figure 3. (a) Experimental two-dimensional (2D) ^{15}N CSA exchange spectra of ^{15}N-aPAN from −60 to 140 °C. Twenty-nine contour lines are plotted between 2 and 30% of the maximum intensity for the spectra from −60 to 120 °C. For the spectra of 130 and 140 °C, 29 contour lines are plotted between 6 and 90%.

exchange signals are observed at 20 °C. Though overlapped with the feet of the dominant diagonal ridges, they are seen to be slightly larger than those at −60 °C. This indicates the presence of relatively slow (τ_c > 0.1 ms) small-angle motions.

Although these 2D NMR spectra show indications of small-angle motions, the spectral changes are quite minor. To confirm the existence of the slow small-angle motions, a 2D pure-exchange (PUREX) experiment was carried out. As described briefly above, 2D PUREX experiments are designed to eliminate the unwanted diagonal ridge so as to clearly reveal off-diagonal exchange signals. Figure 4a shows the experimental PUREX spectrum of a ^{15}N-aPAN sample at 20 °C. The diagonal ridge is suppressed, and the off-diagonal signals near the diagonal are detected clearly, which

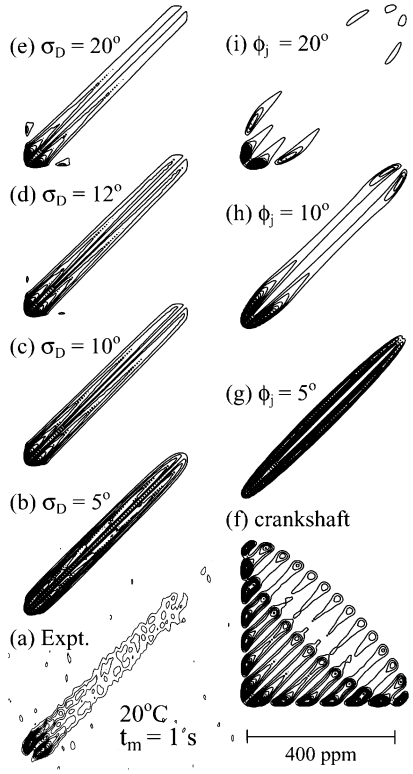

Figure 4. (a) Experimental 2D ^{15}N pure-exchange (PUREX) spectrum of ^{15}N-aPAN at 20 °C. Seventeen contour lines are plotted between 6 and 97% of the maximum intensity. (b−i) Corresponding simulations. Principal values of 144.7 and −289.3 ppm are used for $\sigma_\perp$ and $\sigma_{||}$, respectively, by assuming the ^{15}N CSA is in the rigid limit at −60 °C. (b−e) Simulations based on the amplitude-restricted rotational diffusion motion with distributed amplitude, σ_D, of 5°−20°. The schematics of this model are shown in Figure 10a,c. (f) Simulation for a crankshaft motion. (g−i) Simulations based on two-site exchange motion with a well-defined single amplitude, ϕ_j, of 5°−20°.

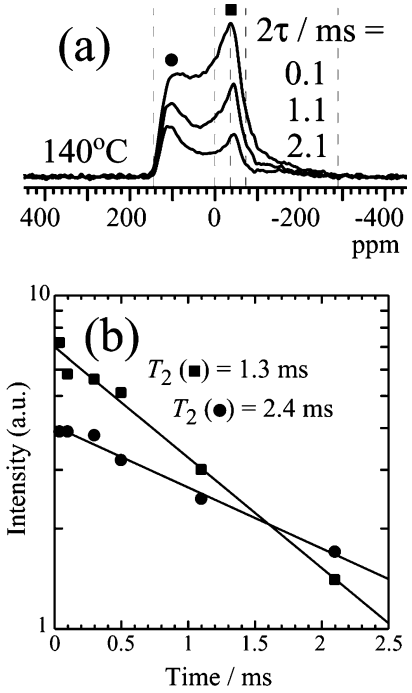

Figure 5. (a) T_2-decay-modulated ^{15}N CSA line shapes of ^{15}N-aPAN at 140 °C. The decay curves corresponding to the chemical shifts near $\sigma_\perp$ (filled circles) and at $-\sigma_\perp/4$ (filled squares) are shown in (b).

confirms the existence of sub-kilohertz small-angle motions in aPAN.

3.2. 1D and 2D ^{15}N NMR: Dynamics above 110 °C. A discontinuous change in 1D ^{15}N CSA line widths and line shapes is observed above ∼110 °C as shown in Figures 1 and 2, indicating the onset of large-amplitude motion.

At 130 °C, an additional signal appears near the isotropic chemical shift and becomes the main peak at 140 °C in Figure 1. This new signal is due to fast motions with larger amplitudes and is most likely related to the change in dielectric relaxation above 110 °C as shown below. Although the chemical shift values of $\sigma_{||}$ are not clear for the spectra at 130 and 140 °C, the chemical shift values of $\sigma_\perp$ are ca. 3.1 and 2.7 kHz, respectively, which is far below the values in Figure 2. From the chemical shift of the new peak, σ_M, the CSA line width is found to be scaled by ca. $-1/4$ compared to the rigid state at −60 °C, that is, $\sigma_M - \sigma_{iso} = -1/4(\sigma_\perp(-60\ °C) - \sigma_{iso})$. The negative prefactor indicates the inversion of the CSA pattern along the *x*-axis of σ_{iso}. A scaling by ca. $\pm 1/4$ was observed previously by ^{2}H NMR experiments on deuterated aPAN samples.[11,27] Although the + and − signs cannot be determined by ^{2}H NMR experiments due to the unavoidable presence of two transitions with positive and negative frequencies in ^{2}H NMR, Thomsen et al.[11] correctly assumed the sign to be negative. From our ^{15}N CSA experiments, which can distinguish the signs, this assumption is proven to be correct.

In Figure 3, the exchange signals are clearly observed over a wider spectral range at higher temperatures up to 120 °C, even without using the PUREX technique. With further increasing temperature, the exchange signals are reduced; see the spectra of 130 and 140 °C. This indicates that the motional rate increases beyond 10 kHz, where the 1D ^{15}N CSA line shapes narrow and the slow-motion condition of 2D exchange NMR is not fulfilled.[28] Note that the diagonal ridge outside of the main motionally narrowed pattern persists. This is a strong indication of segments that do not undergo any large-amplitude motions on any time scale shorter than 1 s.

3.3. T_2-Dependent ^{15}N CSA Spectra. Figure 5 shows the spin−spin relaxation time (T_2) dependence of ^{15}N CSA spectra at 140 °C. The decay curves for the outer peak at −0.6 to −0.8 δ and the inner peak at ca. +0.25 δ result in single-exponential decays with different T_2 values of 2.4 and 1.3 ms, respectively. This might suggest that these peaks correspond to two different morphological components. However, this is not necessarily true. Rather, it is a typical feature of intermediate-rate line shapes[29,30] to show shoulders or peaks at the principal values of both the rigid-limit and the fast-limit tensors. For instance, refs 29 and 30 show differential T_2 across a powder line shape for a single motional process. All the experimental spectra in this work are reproduced by one relatively simple motional process with a moderate distribution of motional amplitudes, as shown in the Discussion section.

3.4. $^{13}CH_2$ Isotropic Chemical Shifts at High Temperatures. On the basis of ^{2}H NMR spectra, Thomsen et al. concluded that aPAN undergoes a crankshaft motion.[11] In their model, all the C−^{2}H bonds undergo the same motion. The crankshaft motion requires a chain structure that would have a gauche

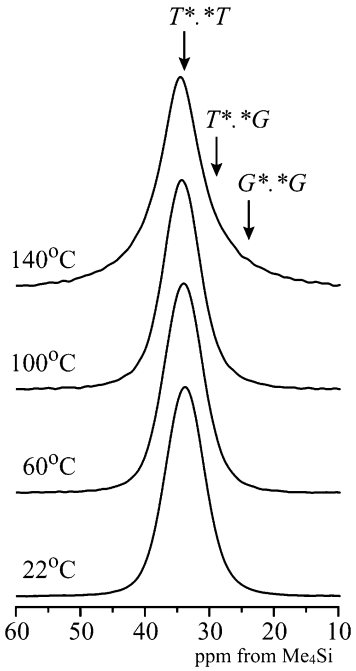

Figure 6. 1D ^{13}C CP/MAS spectra selectively for the methylene groups in aPAN at 22−140 °C. Chemical shifts of several conformations, estimated based on the γ-gauche effect, are indicated in the figure.

content of ∼50% (see discussion below). Therefore, the validity of crankshaft model can be tested by measurements of the trans/gauche ratio of aPAN in the high-temperature range. Our 2D DOQSY experiments[1,2] have revealed a trans/gauche ratio in aPAN of 90:10 (±5)% at 25 °C. It was also found that the γ-gauche analyses[31] are valid for $^{13}CH_2$ resonance lines of aPAN[1] at ambient temperature. Here, trans/gauche ratios of aPAN at elevated temperatures are investigated by γ-gauche analysis of the isotropic chemical shift of the $^{13}CH_2$ resonance line of aPAN. The 1D CP/MAS ^{13}C spectra of the $^{13}CH_2$ units in aPAN are shown in Figure 6. Here, pure CH_2 resonance lines are obtained as described in the Experimental Section. The $^{13}CH_2$ spectra in Figure 6 show no significant chemical shift changes, indicating that the trans/gauche ratios are mostly independent of temperature at least in the measured temperature range. Otherwise, upfield shifts of resonance lines by about 5 ppm are observed for T*.*G conformations. Since the trans/gauche ratio revealed here is quite different from 50:50, a well-defined crankshaft motion can be ruled out.

3.5. Distribution of −C≡N Directions from Static ^{13}C Spectra at 20 °C. The distribution of the directions of −C≡N side groups relative to the macroscopic fiber axis is an important parameter for detailed simulations of the large-amplitude dynamics in aPAN. We characterized this distribution in uniaxially oriented aPAN fibers. Parts a and b of Figure 7 show the experimental 1D CP static ^{13}C spectra of uniaxially oriented aPAN fibers, where the fiber axis is parallel and perpendicular to B_0, respectively. The geometry is shown in the middle of the right column in Figure 7. In Figure 7c, an experimental CSA spectrum of a ^{13}CN-carbon labeled aPAN (^{13}CN-aPAN) sample in the isotropic powdered state is also shown for reference. The CSA frequencies of C≡N carbons spread over the relatively wide chemical shift range of 243 to −120 ppm and the −C≡N side-group directions can be analyzed precisely from CSA

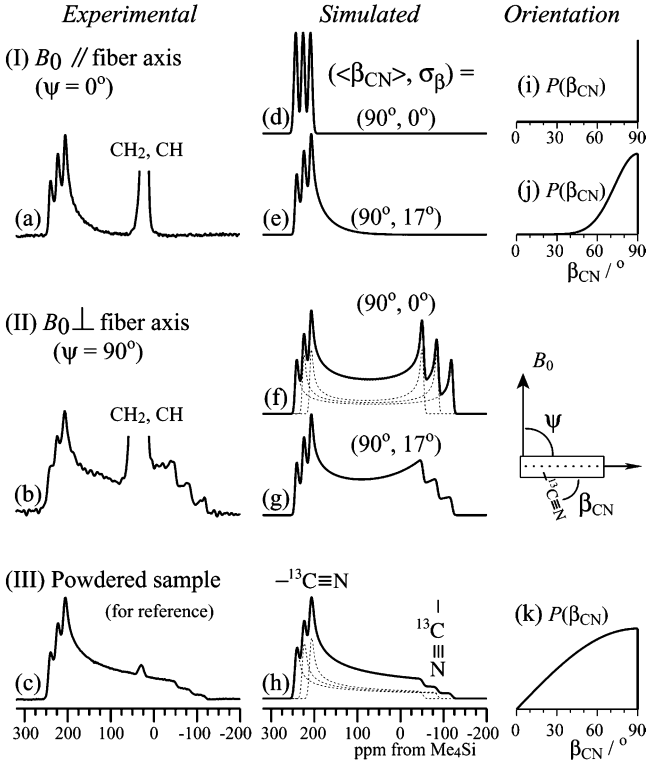

Figure 7. Static ^{13}C CSA spectra of uniaxially oriented aPAN fibers. The geometry is shown in the middle of the right column where the definitions of ψ and β_{CN} are also given. Left column: experimental spectra when (a) B_0 || fiber axis ($\psi = 0°$) and (b) $B_0 \perp$ fiber axis ($\psi = 90°$). The static ^{13}C CSA spectrum of a ^{13}C≡N-labeled aPAN sample in a randomly oriented powdered state is shown in (c) for the reference. Middle column: simulated spectra. The average β_{CN} angle, $\langle\beta_{CN}\rangle$, and the standard deviation σ_β of the Gaussian distribution of β_{CN} angles between the −C≡N bonds and the chain axis are shown in each figure as ($\langle\beta_{CN}\rangle$, σ_β). Three patterns with principal values of ($\sigma_\perp$, $\sigma_\parallel$) = (243, −120), (226, −86), and (209, −52) ppm are superimposed. Gaussian broadenings with standard deviations of 4 ppm were applied. (d) Spectrum with ($\langle\beta_{CN}\rangle$, σ_β) = (90°, 0°) for the $\psi = 0°$ sample orientation. The distribution of β_{CN}, $P(\beta_{CN})$, is shown in (i). (e) Best-fit spectrum with ($\langle\beta_{CN}\rangle$, σ_β) = (90°, 17°) for $\psi = 0°$. The corresponding distribution $P(\beta_{CN})$ is shown in (j). (f) and (g): Simulations corresponding to (d) and (e), respectively, for the $\psi = 90°$ sample orientation. The simulations for (c) and the β_{CN} values are given in (h) and (k).

patterns of C≡N carbons. The simulation for the powdered sample in Figure 7h gives the chemical shift principal values of 243, 226, and 209 ppm for perpendicular alignment of CN groups relative to B_0 and −52, −86, and −120 ppm for parallel alignment of CN groups relative to B_0. The splitting into three lines originates from the dipolar coupling to the directly bonded ^{14}N ($m = -1, 0, +1$ states of spin $L = 1$) as already shown in our preceding paper.[2] In the simulations of Figures 7 and 8, the resonance lines of aliphatic carbons, at about 0−70 ppm, are neglected.

In Figures 7d−g, simulated ^{13}C CSA spectra of uniaxially oriented aPAN fibers are shown. Here, the parameter set ($\langle\beta_{CN}\rangle$, σ_β) is used for the description of the orientation distribution. The average −C≡N direction makes an angle $\langle\beta_{CN}\rangle$ with the fiber axis and the Gaussian distribution around $\langle\beta_{CN}\rangle$ has a standard deviation of σ_β. Figures 7d−g shows simulations under the assumption that the average −C≡N direction is perpendicular to the fiber axis; $\langle\beta_{CN}\rangle = 90°$. A simulation with a single CN side-group direction, ($\langle\beta_{CN}\rangle$, σ_β) =

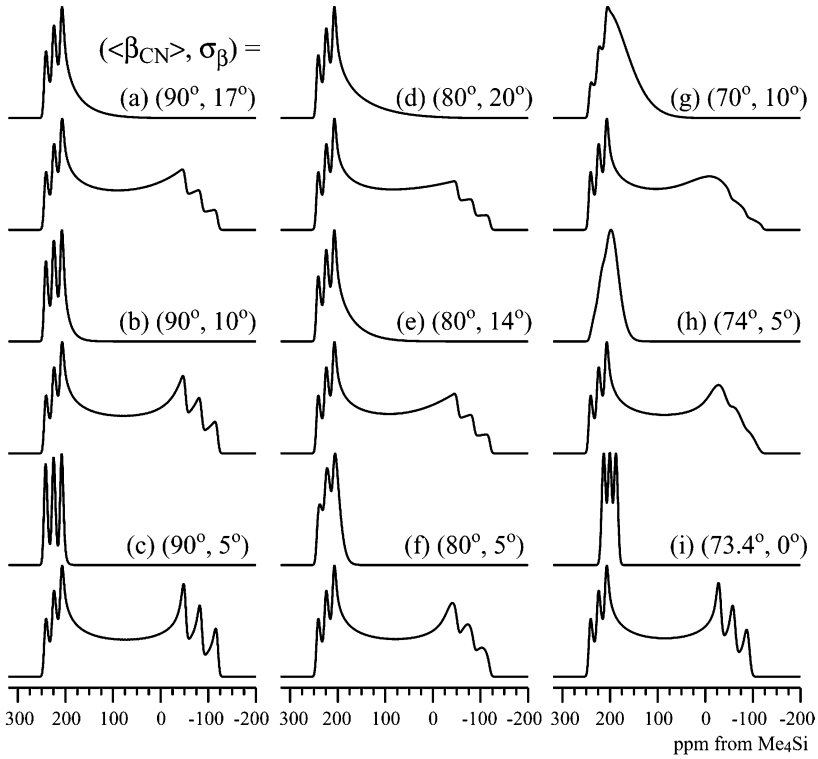

Figure 8. Simulated spectra for the experimental spectra in Figure 7a,b. The values of ($\langle\beta_{CN}\rangle$, σ_β) are shown in each plot. The best fits are obtained in (a) and (e).

(90°, 0°), is shown in Figure 7d for the fiber axes aligned parallel with B_0. Without the distribution, the −C≡N direction is exactly perpendicular to B_0, giving three sharp resonance lines at 243, 226, and 209 ppm. The triplet is due to the dipolar coupling of the ^{13}C nuclear magnet to the ^{14}N nucleus with $m = -1$, 0, and +1, as described above.

The best-fit simulation for Figure 7a is given in Figure 7e. The distribution of −C≡N directions around the average has a standard deviation of $\sigma_\beta = 17°$.[32] Simulations for the perpendicular alignment of the fiber axes relative to B_0 are shown in parts f[33] and g of Figure 7 for ($\langle\beta_{CN}\rangle$, σ_β) = (90°, 0°) and (90°, 17°), respectively. The simulation in Figure 7g with $\sigma_\beta = 17°$, i.e., with the same distribution as in Figure 7e, also well reproduces the experimental spectrum of Figure 7b. The angular distributions of −C≡N groups for the simulated spectra of Figure 7d (and f), e (and g), and h are shown in Figure 7i, j, and k, respectively.

The above simulations assumed that the −C≡N bonds are on average perpendicular to the fiber axis, $\langle\beta_{CN}\rangle = 90°$. In Figure 8, simulated spectra without this assumption are shown. From these simulated spectra, it is found that the experimental spectra are reproduced even when the average −C≡N direction is not exactly perpendicular to the fiber axis. The spectrum in Figure 8e with ($\langle\beta_{CN}\rangle$, σ_β) = (80°, 14°) also reproduces the experimental spectra.

For the simulations of the high-temperature 1D and 2D ^{15}N NMR spectra, we will consider a motional process in which a given −C≡N direction dynamically explores all β_{CN} values in the orientation distribution. The spectral narrowing factor ("−C≡N bond order parameter") S_{CN} as a result of this β_{CN}-averaging motion combined with unrestricted uniaxial rotation (the details of the motions are described later and in Figure 10) is reduced by a factor of f_n from the bond order parameter of a C≡N group oriented at 90° from the uniaxial-rotation axis:

$$S_{CN} = -\frac{1}{2} f_n \tag{3a}$$

$$= \frac{1}{2}\langle 3\cos^2\beta_{CN} - 1\rangle \tag{3b}$$

$$= \int_{0°}^{90°} P(\beta_{CN})\frac{1}{2}(3\cos^2\beta_{CN} - 1)\, d\beta_{CN} \tag{3c}$$

$$= \frac{1}{\delta}\int_{-\delta/2}^{\delta} S_{||}(\omega_a)\omega_a\, d\omega_a \tag{3d}$$

where $\omega_a = \omega - \omega_{iso}$ is the anisotropic frequency of eq 1, and $S_{||}(\omega_a)$ is the spectrum obtained with the fiber axes parallel to B_0. In this model, a given aPAN chain does not only rotate around its axis but also flexes within the channel formed by its six neighbor chains (see Figure 10a); this moves a given C≡N bond through the full range of possible orientations relative to the channel axis. Some examples of $P(\beta_{CN})$ are shown in the right column of Figure 7. Figure 9 shows the dependence of f_n on the width σ_β of the $P(\beta_{CN})$ distribution for several $\langle\beta_{CN}\rangle$ values. The f_n value of 0.754 calculated directly from the experimental ^{13}C spectrum according to eq 3d is also indicated; the aliphatic signals were subtracted from the experimental spectrum before the integration. The figure shows that f_n does not determine the parameter set ($\langle\beta_{CN}\rangle$, σ_β) uniquely. However, the experimental $f_n = 0.754$ is seen to set an upper limit of 17° for σ_β and a lower limit of 73.4° for $\langle\beta_{CN}\rangle$. In addition, spectra simulated for $\langle\beta_{CN}\rangle < 78°$ do not reproduce the experimental spectra in Figure 7a,b; for instance, the simulated spectra for ($\langle\beta_{CN}\rangle$, σ_β) = (74°, 5°) and (73.4°, 0°), both with $f_n = 0.754$, are different from the experimental spectra, as shown in Figure 8h,i. Therefore, we can

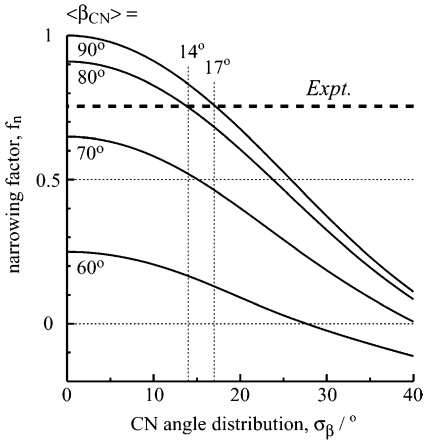

Figure 9. Dependence of narrowing factors, f_n, by dynamic β_{CN}-averaging (δ-average) on C≡N angles and the distributions. The f_n calculated from the experimental spectrum in Figure 7a, 0.754, is shown as a broken line. The values, σ_β, are found to be 17° and 14° for $\langle\beta_{CN}\rangle$ = 90° and 80°, respectively.

conclude that the distribution of C≡N directions is between ($\langle\beta_{CN}\rangle$, σ_β) = (90°, 17°) and (80°, 14°).

In the 1D ^{15}N CSA spectra at 130 and 140 °C, a peak, presumably at $\omega_{iso} - \delta/2$, is observed at $-\sigma_\perp/4$ in Figure 1a. The model of fast dynamic β_{CN}-averaging motion (see Figure 10a) as described in the previous paragraph is needed to describe the strong motional narrowing in this temperature range. If the β_{CN}-averaging motion did not occur, the spectra would be broadened as described later. The fast-motion limit of this β_{CN}-averaging motion is equivalent to a uniaxial motion with an effective angle β_{CN}^{eff} between the rotation axis and the C≡N bond direction defined by

$$S_{CN} = \frac{1}{2}\langle 3\cos^2\beta_{CN} - 1\rangle = \frac{1}{2}(3\cos^2\beta_{CN}^{eff} - 1) \quad (4)$$

We use the value of $\beta_{CN}^{eff} = 73.4°$, calculated from $f_n = 0.754$, in the following simulations at high temperatures. According to a previous infrared dichroism study of uniaxially drawn aPAN by Bashir et al.,[34] the most appropriate angle between C≡N bonds and chain axis is 73°. (A distribution of angles was not considered in that study.) This value is in excellent agreement with our result, $\beta_{CN}^{eff} = 73.4°$. Note that $\beta_{CN}^{eff} \neq \langle\beta_{CN}\rangle$ if the distribution is not a delta function: Because of the nonlinearity of $(3\cos^2\beta_{CN} - 1)$, we have in general that

$$\langle 3\cos^2\beta_{CN} - 1\rangle \neq 3\cos^2\langle\beta_{CN}\rangle - 1 \quad (5)$$

which, combined with eq 4, proves $\beta_{CN}^{eff} \neq \langle\beta_{CN}\rangle$.

The value of $f_n = 0.754$ results in a C≡N bond order parameter $S_{CN} = -1/2 f_n = -0.377$. This is larger than the value of $-1/4$ obtained from the peak maximum position in Figure 1a. However, $-1/4$ will be obtained only in the fast limit and with full (amplitude-unrestricted) rotational diffusion. The following simulations based on our model give the δ-averaged peak at the correct position (see Figure 17 below). This shows that the dynamic averaging within the experimentally determined C≡N orientation distribution is consistent with the high-temperature spectra. Further analysis and discussion follows below.

3.6. Dielectric Experiments. Figure 11 shows the frequency dependence of dielectric loss, ϵ'', for aPAN in the temperature range from 15 to 130 °C. It is found that ϵ'' gradually increases with increasing temperature below 110°C. Above 110 °C, ϵ'' increases steeply and shows a clear maximum for each temperature. This is

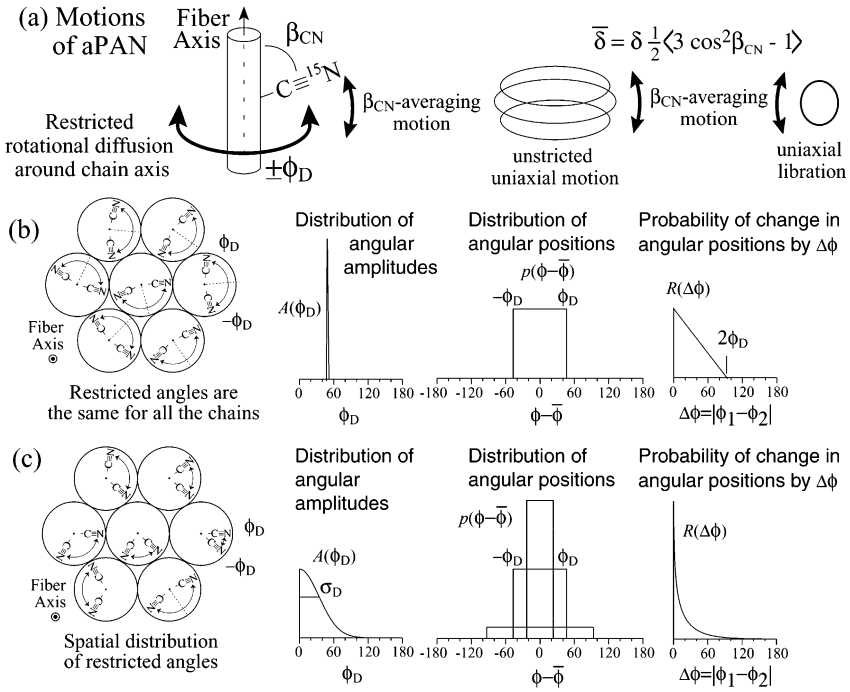

Figure 10. Schematic representation of the motional model of aPAN. (a) Uniaxial rotational diffusion around the fiber axis with restricted amplitude ϕ_D. The β_{CN}-averaging motion, which would occur simultaneously with rotational diffusion motion, is also shown. (b) Amplitude-restricted rotational diffusion with a single amplitude ϕ_D. The spectra in Figure 15 are based on this model. The corresponding reorientation-angle distribution $R(\Delta\phi)$ for long mixing times is also shown. (c) Amplitude-restricted rotational diffusion with distributed amplitudes. The standard deviation of the amplitude distribution $A(\phi_D)$ is denoted as σ_D. The corresponding reorientation-angle distribution $R(\Delta\phi)$ for $t_m \gg \tau_c$ is also shown. While $A(\phi_D)$ and $R(\Delta\phi)$ have been represented accurately, the superposition of the distributions of angular positions $p(\phi - \bar{\phi})$ (which are different for different sites and should not be added up) is shown only schematically. The spectra in Figures 4b−e, 16, and 17 are based on this model.

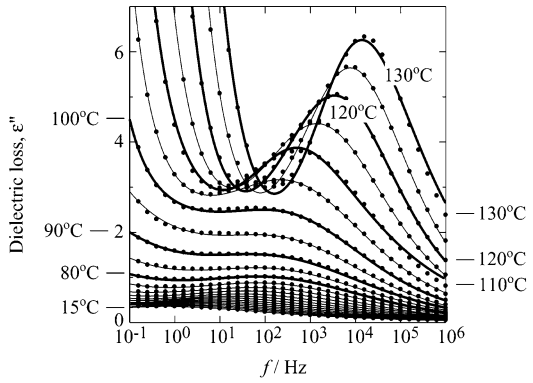

Figure 11. Frequency dependence of the dielectric loss ϵ'' for aPAN. Solid lines are fits to the Havriliak−Negami function, $\epsilon^*(\omega) = \epsilon'(\omega) - j\epsilon''(\omega) = \Delta\epsilon/\{1 + (j\omega\tau_{HN})^{\beta}\}^{\alpha} + \sigma_{DC}/j\omega\epsilon_0 + \epsilon_\infty$, where $\epsilon^*(\omega)$ is the complex permittivity, $\epsilon'(\omega)$ the real part of the dispersion, $\epsilon''(\omega)$ the imaginary part, ϵ_∞ the dielectric constant at $\omega \rightarrow \infty$, $\Delta\epsilon$ the relaxation strength, τ_{HN} the characteristic relaxation time of the Havriliak−Negami equation, ϵ_0 the dielectric constant of vacuum, j the imaginary unit, and σ_{DC} the dc conductivity. The variables α and β are empirical parameters, and the values are in the range of 0.27−0.57 and 0.47−1.0, respectively, depending on the temperatures.

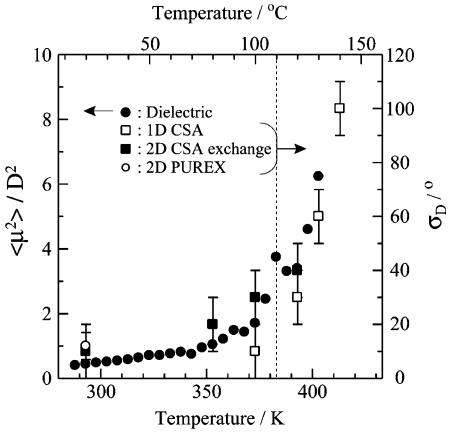

Figure 12. Mean-square dipole moment $\langle\mu^2\rangle$ of aPAN (filled circles), calculated from the dielectric data of Figure 11 by using Onsager's equation. The widths σ_D of the distributions of amplitudes of motion obtained from 1D CSA, 2D exchange, and 2D PUREX NMR experiments are also shown as open squares, filled squares, and an open circle, respectively.

in good agreement with the increasing amplitude and rate in the ^{15}N NMR data of Figures 1a and 2.

The filled circles in Figure 12 show the temperature dependence of the mean-square dipole moment, $\langle\mu^2\rangle$, calculated from Figure 11 by using Onsager's equation

$$\langle\mu^2\rangle = \frac{9kT}{4\pi N}\frac{\Delta\epsilon(2\Delta\epsilon + 3\epsilon_\infty)}{(\Delta\epsilon + \epsilon_\infty)(\epsilon_\infty + 2)^2} \qquad (6)$$

where N is the number of dipoles per unit volume and k is the Boltzmann constant. The density of aPAN, 1.17−1.22 g cm^{-3},[1-3] and the molecular weight of monomer unit, 53.05, are used for the calculation of the value of N. The quantities $\Delta\epsilon$ and ϵ_∞ are the relaxation strength of the sample and the dielectric constant at $\omega \rightarrow \infty$, respectively. In contrast to its gradual increase below 110 °C, $\langle\mu^2\rangle$ rapidly increases at higher temperatures. This is quite similar to the trend in Figure 2 and indicates that the amplitude of −C≡N group motion increases quite suddenly above 110 °C. The dielectric

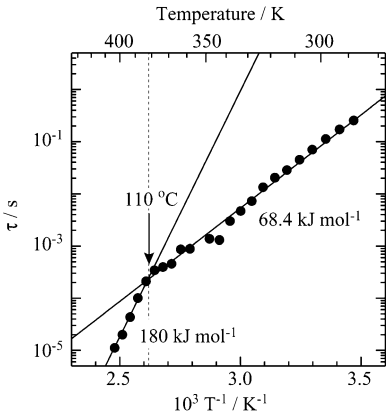

Figure 13. Arrhenius plot of the correlation (or relaxation) time of motion in aPAN, obtained from the dielectric data of Figure 11. Two different activation energies, 68.4 and 180 kJ mol^{-1}, are obtained for the low- and high-temperature sides of the relaxation, respectively.

experiments cannot distinguish whether the increase of $\langle\mu^2\rangle$ originates from the increase of the amplitude of motion or of the fraction of mobile components. From the quantitative analysis of NMR data, an increase of the amplitude of motion is found to be responsible (see below).

In Figure 13, the correlation or relaxation time, calculated from the inverse of the frequency of the loss maximum, $\tau = (2\pi f_{max})^{-1}$, is plotted against the inverse absolute temperature, T^{-1}. This shows a clear inflection at 110 °C. In each temperature region, the experimental data follow an Arrhenius relation; the activation energies below and above 110 °C are determined to be 68.4 and 180 kJ mol^{-1}, respectively. This indicates that the relaxation at 110 °C does not correspond to a glass transition; otherwise, the data should follow a WLF type relation. These dielectric results are in good agreement with those obtained here by NMR.

4. Discussion

4.1. Low-Temperature Motions. The WAXD pattern of this aPAN sample shows pseudohexagonal chain packing. Moreover, our previous investigations,[1,2] the above-mentioned 1D ^{13}C CP/MAS experiments on a powdered sample, and the static ^{13}C experiments on uniaxially oriented fibers have revealed that (i) the trans/gauche ratio in aPAN is 90:10 and (ii) the −C≡N directions are approximately perpendicular to the fiber axis, typically ($\langle\beta_{CN}\rangle$, σ_β) = (90°, 17°). These results suggest that the most likely motional process is a rotation around the chain axis.

Figure 14a−g shows simulated 2D exchange spectra for two-site exchange motion with a well-defined single amplitude, ϕ_j. Spectra with distributed β_{CN} angles of ($\langle\beta_{CN}\rangle$, σ_β) = (90°, 17°) are summed up for each simulation. Simulated spectra with a single effective β_{CN} angle, β_{CN}^{eff} = 73.4°, give indistinguishable patterns (not shown here). This means that this experiment is insensitive to the β_{CN}-averaging motion, and the amplitude of rotational motions around the chain axis can be determined regardless of whether β_{CN}-averaging motions occur or not. The elliptical exchange patterns that are clearly visible in these simulations are not observed in the experimental spectra in Figure 3. Instead, the intensities continuously decrease from the diagonal in the experimental spectra, which indicates that there is

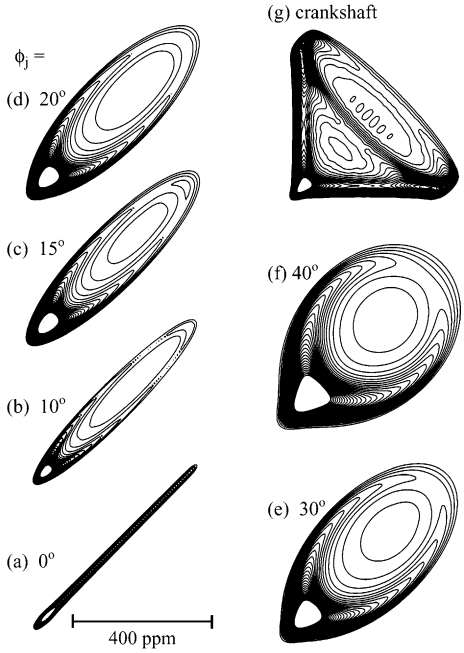

Figure 14. Simulated two-dimensional (2D) ^{15}N CSA exchange spectra of ^{15}N-aPAN under two-site exchange motion with a well-defined single amplitude, ϕ_j, of 0°−40° in (a)−(f). A simulation for a crankshaft motion is shown in (g). Rigid-limit principal values of 144.7 and −289.3 ppm are used for $\sigma_\perp$ and $\sigma_{||}$, respectively, based on the ^{15}N CSA at −60 °C.

a distribution of amplitudes of motion, ϕ_j, that is restricted to small angles.

As a simple but realistic motional model, we consider restricted uniaxial diffusion. The model is shown in Figure 10. In this model, CN groups and therefore aPAN chains undergo restricted rotational diffusion around the chain axes as shown in Figure 10a. Accompanying the dynamics of the CN groups around the chain axis, motional averaging of the angle β_{CN} between the CN bond direction and the chain axis is considered. This motion occurs at least at high temperature, as shown later. For mixing times t_m that are sufficiently long compared to the motional correlation time τ_c, $t_m \gg \tau_c$, the reorientation-angle distribution $R(\Delta\phi)$, which fully determines the 2D exchange patterns, is the autocorrelation function of the distribution $p(\phi - \bar{\phi})$ of angular positions in an ensemble of equivalent segments: A segment starting out at ϕ_1 has a reorientation-angle distribution $p(\Delta\phi + \phi_1)$, and its probability of starting out at ϕ_1 is $p(\phi_1)$. Thus, the overall reorientation angle distribution is

$$R(\Delta\phi = \phi_2 - \phi_1) = \int_0^{2\pi} p(\phi_1)\, p(\Delta\phi + \phi_1)\, \mathrm{d}\phi_1 \quad (7)$$

The $p(\phi - \bar{\phi})$ box function, with equal probability between $-\phi_D$ and $+\phi_D$, thus results in a triangular $R(\Delta\phi)$ as shown in Figure 10b. In this model, all the CN groups undergo motions with the same amplitude ϕ_D. However, the 1D ^{15}N CSA spectra produced by this simple model (see Figure 15) do not reproduce the experimental spectra in Figure 1a.

Because of the configurational and conformational disorder of aPAN, it is reasonable to assume that the amplitudes of the motion for respective CN groups are distributed as shown in Figure 10c. In this model, a Gaussian distribution, $A(\phi_D)$, is assumed for the motional amplitude ϕ_D. Its maximum is at $\phi_D = 0$, and the

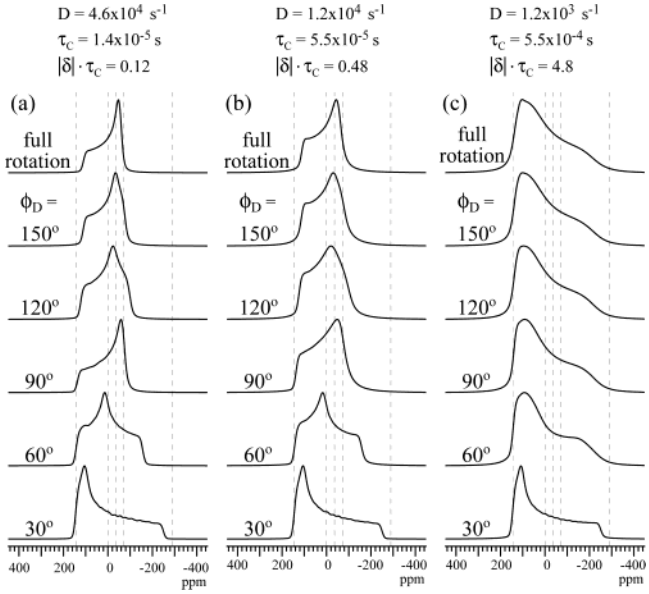

Figure 15. Simulations of 1D ^{15}N CSA spectra for amplitude-restricted uniaxial rotational diffusion. The schematics of this model are shown in Figure 10a,b. The diffusion coefficients, D, are (a) 4.6×10^4 /s, (b) 1.2×10^4 /s, and (c) 1.2×10^3 /s. The motional rates are shown at the top of figure by three different expressions: the diffusion coefficient D, the correlation time, τ_c, and the unitless product $|\delta|\tau_c$ where $|\delta|$ is the ^{15}N CSA (or ^{2}H quadrupolar) anisotropy parameter. The amplitudes are shown for each figure. The simulations of free rotational diffusion, i.e., with unrestricted amplitude, are also shown at the top of each column.

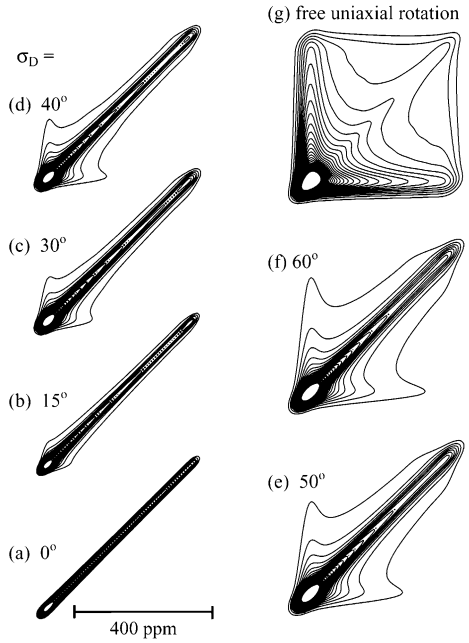

Figure 16. Simulated 2D ^{15}N CSA exchange spectra of ^{15}N-aPAN under amplitude-restricted uniaxial rotational diffusion motion with distributed amplitude, σ_D, of 0°−60° in (a)−(f). The schematics of this model are shown in Figure 10a,c. A simulation for a free (amplitude-unrestricted) uniaxial rotational diffusion motion is shown in (g).

standard deviation of this distribution is defined as σ_D. The function $R(\Delta\phi)$ is now obtained by summation of triangular $R(\Delta\phi)$ functions for each ϕ_D value. The $R(\Delta\phi)$ thus obtained is shown in Figure 10c. Figure 16 shows simulated spectra based on this distribution $R(\Delta\phi)$. The simulations reproduce the experimentally observed continuous intensity decrease from the diagonal (see

Figure 3). The widths σ_D of the amplitude distribution are determined to be 10°, 20°, 30°, and 40° with an uncertainty of ~±7° for the spectra taken at 20, 80, 100, and 120 °C, respectively, for the correlation time of ~1 s. In contrast, simulations based on Gaussian shapes of $R(\Delta\phi)$ (rather than $A(\phi_D)$) do not reproduce the experimental 2D exchange spectra in Figure 3.

Simulated 2D PUREX spectra, to be compared with the experimental pattern in Figure 4a, are displayed in Figure 4b−i. They again are based on models of rotational motion around the chain axis. Simulations based on two-site exchange motion with a well-defined single amplitude, ϕ_j, as shown in Figures 4g−i, fail to reproduce the experimental spectrum of Figure 4a. Simulations based on the model in Figure 10c, with a Gaussian distribution of amplitudes of unixial rotation diffusion, are shown in Figure 4b−e. The two straight ridges parallel to the diagonal in Figure 4a are well reproduced by the simulation in Figure 4d. This again confirms that the model of Figure 10c. The value of σ_D is determined to be 12 ± 5° for the mixing time of 1 s at 20 °C. In all the PUREX simulations, the Gaussian β_{CN} angle distributions characterized by $(\langle\beta_{CN}\rangle, \sigma_\beta) = (90°, 17°)$ are considered; simulations with distributed β_{CN} angles and with a single angle β_{CN}^{eff} are indistinguishable also for 2D PUREX simulations.

The experimental 2D exchange spectra in Figure 3 exclude uniaxial rotational diffusion of unrestricted amplitude at temperatures below 120 °C. The signal intensity in the experimental spectra clusters around the diagonal, which is inconsistent with the simulation for free uniaxial rotational diffusion in Figure 16g. Therefore, the amplitudes of rotational motion around the chain axis are found to be very limited at least below 120 °C.

4.2. High-Temperature Fast Uniaxial Rotational Diffusion and Dynamic β_{CN}-Averaging. From the above analysis of the 2D NMR data, −C≡N groups are found to rotate around the fiber axis. The rotation is not free; i.e., the amplitude of motion is restricted. Correspondingly, we have simulated the high-temperature 1D ^{15}N spectra in terms of restricted uniaxial rotational diffusion around the fiber axis. The motion, which corresponds to the restricted diffusion model in ref 35, is schematically shown in Figure 10a,b. The simulation was performed with an exchange-matrix treatment of a large number of discrete orientational sites, N, separated by a rotation angle ϵ and spread over an arc of $2\phi_D$. Here, $\epsilon = 2\phi_D/(N - 1)$. The diffusion coefficient is related to the jump rate by $D = \epsilon^2\kappa$, where κ is defined as the jump rate to the nearest-neighboring sites. The diffusion coefficient D is related to the intrinsic correlation time, τ_c, by $\tau_c = (\pi^2/15)(1/D) = 0.66/D$.[35,36]

The simulated spectra are shown in Figure 15. The dependence of the spectral patterns on the amplitude of motion, ϕ_D, is clearly seen. On this basis, the amplitude of motion can be estimated from the experimental 1D CSA spectra. The spectral patterns are gradually broadened with increasing τ_c, and the spectral patterns change significantly at $|\delta|\tau_c \sim 1$ for large-amplitude motions. Therefore, for large-angle motions we can determine whether $|\delta|\tau_c$ exceeds ~1 or not. For small amplitudes, the spectral patterns are quite insensitive to τ_c, and we cannot determine τ_c for small-angle motions. Spectra with any value of $|\delta|\tau_c < 0.1$ are in the fast-motion limit and indistinguishable; similarly, τ_c cannot be determined from 1D line shapes in the slow limit, $|\delta|\tau_c > 10$.

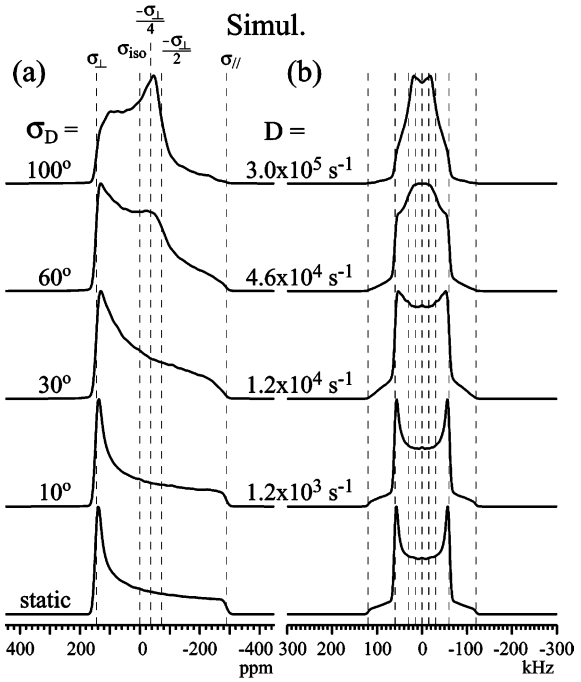

Figure 17. (a) Best-fit simulations of the experimental 1D ^{15}N CSA spectra of Figure 1a, based on the model of uniaxial rotational diffusion with distributed restricted amplitudes. This model is represented schematically in Figure 10a,c. The width σ_D of the amplitude distribution and the diffusion coefficients D are shown for each figure. The corresponding correlation times are $\tau_c = 2.2 \times 10^{-6}$, 1.4×10^{-5}, 5.5×10^{-5}, and 5.5×10^{-4}, and the unitless products are $|\delta|\tau_c = 0.019$, 0.12, 0.48, and 4.8, from the highest spectrum. Note that σ_D is determined quantitatively but D (and therefore τ_c) is not determined uniquely by this experiment as described in section 4.2. (b) Corresponding symmetrized simulations. The ^{15}N chemical shift in kilohertz has been multiplied by 13.6 in order to produce the corresponding ^{2}H quadrupolar frequency. Finite-pulse-width corrections have been applied to make the symmetrized ^{15}N spectra directly comparable with the ^{2}H spectra in ref 11.

No simulations with a single motional amplitude ϕ_D in Figure 15 reproduce the experimental spectra above 120 °C. Figure 17 shows best-fit spectra for the experimental line shapes of Figure 1. These simulations are obtained in terms of the model in Figure 10c by summing up subspectra with various ϕ_D values, weighted by a Gaussian distribution $A(\phi_D)$ of standard deviation σ_D. This model, shown in Figure 10a,c, means that some CN groups move with larger angles, others with smaller angles, around the chain axis. This motional heterogeneity would result from the disordered structure of aPAN.

The persistent diagonal ridge in the 2D spectra even at high temperatures provides strong support for this model, which attributes the superposition of more and less motionally narrowed line-shape components to a distribution of amplitudes rather than a distribution of correlation times. The diagonal ridge tells us that the less mobile segments, which contribute to the broad portion of the 1D line shape that resembles the low-temperature spectrum, do not undergo large-amplitude motions on a 1 s time scale. Since the majority of the segments undergo fast motions, $\tau_c < 3 \times 10^{-4}$ s, the segments that do not reorient on the 1 s time scale cannot be simply the slow tail of a distribution of

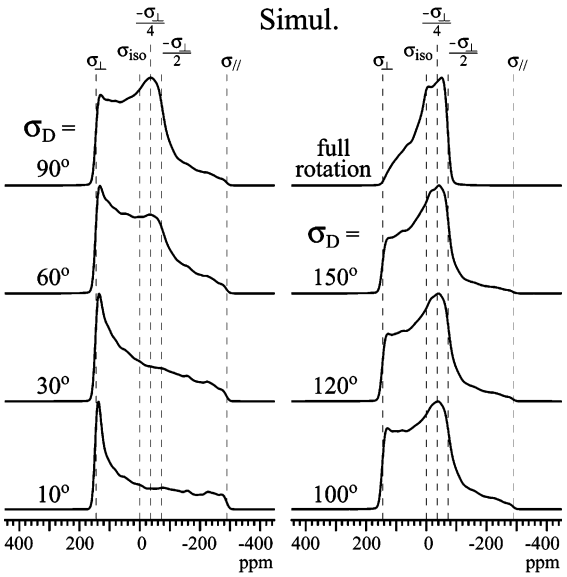

Figure 18. Simulations of 1D ^{15}N CSA spectra based on the model of uniaxial rotational diffusion with distributed restricted amplitudes, as shown in Figure 10a,c, but without the β_{CN}-averaging motion included in the simulations of the spectra in Figure 17. A diffusion coefficient of $D = 3.0 \times 10^5$ s^{-1}, which corresponds to $\tau_c = 2.2 \times 10^{-6}$ s and $|\delta|\tau_c = 0.019$, is used for all the simulations. The width σ_D of the amplitude distribution is shown for each figure.

correlation times (unless the distribution is $\pm 4 = 8$ decades wide, which is unrealistic and inconsistent with the drastic changes of the line shape with temperature). Note that the distribution of amplitudes does not necessarily mean that the heterogeneity originates from morphologically different phases. The distribution of motional amplitudes is described by a single Gaussian distribution $A(\phi_D)$, not by a combination of two different Gaussian distributions, at any temperature. The best-fit simulations in Figure 17 were obtained with σ_D values of 10°, 30°, 60°, and 100° for the spectra at 100, 120, 130, and 140 °C, respectively.

For all the 1D CSA simulations in Figures 15 and 17, the effective β_{CN} value of 73.4° is used in order to reduce the simulation time. Like the 2D spectra, the 1D line shapes with and without β_{CN}-averaging are indistinguishable for temperatures below ~120 °C. Above that temperature, the β_{CN}-averaging motion is considered to accompany with rotational motion around the chains. A simulation without β_{CN}-averaging is different from the experimental spectra at 140 °C (see Figure 18 with $\sigma_D > 90°$) in that the main peak is broadened. The wiggles on the simulated spectra in Figure 18 are numerical noise.

4.3. A Glass Transition in PAN ? Our NMR and dielectric data indicate that the amplitude and rate of the motion around the fiber axis increases strongly between 90 and 120 °C. The amplitudes obtained from the 1D and 2D NMR results are plotted as a function of temperature in Figure 12. The temperature change is in good agreement with that of the dielectric strength. This indicates that the increase of $\langle\mu^2\rangle$ originates from an increase of the amplitude of motion, not from an increase of the fraction of mobile segments.

The 1D NMR spectra for a wide range of correlation times are indistinguishable; only a lower limit of τ_c can be provided. However, the results are consistent with the dielectric data in Figure 13. On the other hand, the dielectric results reported above seem to contradict the analysis of Gupta and Chand (see Figure 4 in ref 18), who interpreted their data not in terms of two Arrhenius relations but by using the WLF relation. However, ref 18 shows only four data points. If our plot had only four data points covering both temperature regions, it could in fact also be fitted with a WLF curve. Gupta and Chand also plotted previously reported data by Hayakawa et al.,[16] Saito and Nakajima,[15] and Ishida et al.[19] and fit their data by WLF curves. However, Hayakawa et al.[16] clearly rejected the possibility of a glass transition in their original paper (see the discussion in ref 16). The data by Saito and Nakajima[15] and by Ishida et al.[19] clearly follow the Arrhenius relation. In conclusion, it does not appear correct to assign this motion to a glass transition.

The activation energies obtained in our work are in agreement with the previous data; 86.2[37] and 59[19] kJ mol^{-1} were reported for the lower temperature region and 167[19] and 222[19,38] kJ mol^{-1} for the higher temperature region. Note that the transition temperatures are not always consistent; the temperatures are 108,[37] 140,[19] and 63 °C.[19,38] The difference could originate from the differences of measurements and sample preparations. The dynamic modulus (230−290 cps) was measured on drawn fiber samples,[37] and dielectric loss measurements (0.1−1000 kc/s) were carried out on cast films[19] and single-crystal mats.[19,38] In any case, our activation energies of 68 and 180 kJ mol^{-1} for the lower and higher temperature regions, respectively, are within these previously reported values.

4.4. Critical Discussion of the Crankshaft Model. On the basis of their ^{2}H NMR data, Thomsen et al. proposed that aPAN chains undergo a crankshaft motion. The crankshaft is thought to consist of five backbone bonds with the conformation of TGTGT.... This conformation makes the G bonds parallel to the fiber axis, and the motion occurs around the parallel bonds. The 50:50 T/G ratio in the crankshaft model is inconsistent with the experimentally determined 90:10 ratio in refs 1, 2, and 10 and with the CP/MAS results shown above. It also does not agree well with the C≡N orientation distribution measured above (Figure 6). The crankshaft motion of Thomsen et al. consists of 120° jumps of C−^{2}H bonds on a cone with an opening angle of 66° (modified from the ideal 70.5°, which does not produce a sufficiently small averaged quadrupolar splitting). This is a significantly smaller cone apex angle than the >73° determined above for the C≡N groups, which are orienationally almost equivalent to the deuterons.

The 2D exchange experiments show additional critical differences. If the motion is also present at lower temperatures, well-defined elliptical ridges will be observed by 2D CSA exchange experiments, similarly as, for example, for the 200° rotation helical jumps in poly(oxymethylene) or the ~100° rotation helical jumps in poly(ethylene oxide), both of which involve gauche conformations. In the present crankshaft model, clear elliptical ridges for ~110° rotation[39] are expected as well for the 2D exchange spectra (see Figure 14g). The 2D exchange experiments observe slower motion (on the order of milliseconds to seconds) compared to that of 1D line shape analyses; thus, the corresponding motion will be observed at a lower temperature range. However, the experimental 2D ^{15}N PUREX spectrum in Figure 4a and 2D ^{15}N CSA exchange spectra in Figure 3 do not give

elliptical ridges characteristic of the crankshaft motion as shown in Figures 4f and 14g.

Note that the crankshaft motion proposed for aPAN by Thomsen et al. and considered in this study is not a defect running through the polymer chains but the motion of translationally stationary sections of the chain. We do believe that traveling defects are responsible for producing the rotational diffusion and β_{CN}-averaging motion described in section 4.2. It may be instructive to compare the situation in aPAN to the case of orthorhombic polyethylene (PE). The PE chains in the crystallites undergo 180° flips,[40] which are now widely accepted as closely related to the α_C relaxation. The defect motion involves a complex distortion of the PE chain,[41−43] while the simplified description in terms of 180° flips involves only all-trans conformations. Similarly, traveling defects in aPAN are also expected to involve significant distortions from the predominantly trans equilibrium structure of aPAN. The observable motion in PE is the 180° flip, while the defect motion is very difficult to observe. In the same sense, the observable motion in aPAN is rotational diffusion (and the β_{CN}-averaging motion), while the traveling defects are too short-lived to be accessible to NMR analysis.

4.5. Motional Process in the High-Temperature Range: Comparison of ^{15}N and ^{2}H NMR. In the above discussion, we found that the crankshaft model is inconsistent with the experimental data up to 140 °C. However, another relaxation at about 140 °C is frequently observed for aPAN. Therefore, there is a possibility that the crankshaft motion occurs above that temperature, since Thomsen et al. carried out the simulations based on the crankshaft motion for their experimental ^{2}H NMR spectra above 150 °C. To directly compare ^{15}N CSA spectra in Figure 1a and ^{2}H spectra in ref 11, we have symmetrized our experimental ^{15}N spectra (see Figure 1b) to create patterns equivalent to ^{2}H spectra.[44] The visual comparison of ^{2}H and ^{15}N spectra is much facilitated by the symmetrized presentation. The widths of the rigid-limit ^{15}N CSA and ^{2}H Pake patterns are different by an order of magnitude; the value of $|\delta|$ is about 289 ppm (8.8 kHz at a Larmor frequency of 30.4 MHz) for ^{15}N CSA spectra, while the quadrupolar coupling parameter (splitting) is 120 kHz for ^{2}H NMR spectra. This means that motions with 13.6 times lower rates are observable in our ^{15}N experiments. This results in different temperatures for similar line shape changes in the two NMR experiments. From the activation energy of 180 kJ mol^{-1} obtained from the dielectric data and considering the 13.6-fold difference in the ^{15}N and ^{2}H NMR frequencies, the difference of $1000/T$ is calculated to be 0.121.[45] This corresponds to a ∼20 K shift in the temperature range of 100−140 °C in ^{15}N line shapes, relative to the matching ^{2}H line shapes. From the comparison, we find good agreement of the symmetrized ^{15}N spectra in Figure 1b with the ^{2}H spectra of Figure 3 in ref 11, with a consistent 20 °C shift. In the ^{15}N and ^{2}H spectra, the central portion of the spectrum starts to rise at 100 and 120 °C, respectively. The ^{15}N CSA line shapes at 120 and 130 °C are quite similar to the ^{2}H line shapes at 140 and 151 °C, respectively. Line shapes distinctly scaled by $-1/4$ are observed above 140 and 162 °C, respectively. Corresponding simulated spectra based on the amplitude-restricted rotational diffusion motion are shown in Figure 17b. This figure shows that Thomsen's ^{2}H NMR spectra below 162 °C can be explained by our model.

However, the above analysis has a problem. Although there exists a temperature (or a correlation time) shift for ^{15}N and ^{2}H NMR experiments as described above, the amplitude of motion should be the same at the same temperature for both experiments. This means that, for example, the symmetrized ^{15}N spectra at 130 and 140 °C should give a wider pattern compared to ^{2}H spectra at 151 and 162 °C, respectively, due to smaller motional amplitudes. However, the ^{15}N spectra in Figure 1b and ^{2}H line shapes of Figure 3 in ref 11, both experimental spectra, agree well with each other with a consistent 20 °C shift. Several factors can be considered as potential explanations:

(1) Maybe differences in sample preparation affect the motion. For instance, the previously reported dielectric results show significant discrepancies between the temperature dependences of different samples. A typical example is shown in Figure 4 of ref 18. A shift of about 30 °C exists between Gupta's and Hayakawa's data.

(2) Possibly, the amplitude of motion at higher temperature does not increase significantly with temperature beyond the range plotted in Figure 12. Actually, Hayakawa et al.[16] observed such a temperature dependence of relaxation strength in their dielectric measurements. The relaxation strength increases from 40 to 120 °C but starts to level off at higher temperature. Our dielectric data are quite similar to those literature data, although the amplitude appears to continue to increase up to 130 °C.

(3) In NMR experiments, the displayed temperature may differ from the real temperature of the sample, in particular for temperatures far from ambient. The temperatures given in this paper are based on careful calibrations as described in the Experimental Section, and our NMR data are in good accord with our dielectric data. In contrast, there is no description of temperature calibration in the ^{2}H NMR study of ref 11. If the real temperatures of ^{2}H NMR spectra in ref 11 are ∼10 °C lower, our rotational diffusion model reasonably explains their results up to 184 °C. This indicates that in this high-temperature range the character of the motion does not change strongly but that the amplitude and rate simply increase. According to our analysis, the rate goes up with an activation energy of 180 kJ mol^{-1}, while a much smaller activation energy of 45 kJ mol^{-1} was obtained by Thomsen et al. from their high-temperature ^{2}H NMR data. However, this value is inconsistent with all other values in the literature (see above), which suggests a problem with the temperature readings or the analysis in that work.

Note that for the symmetrized ^{15}N spectra in Figures 1b and 17b the chemical shift scale, in kilohertz, is multiplied by 13.6 to give ^{2}H-equivalent patterns. A finite-pulse-width correction, corresponding to the experimental conditions of Thomsen et al., is also applied to these spectra; this is the origin of the noise-free baseline outside of the spectra even for the symmetrized experimental spectra in Figure 1b.

4.6. Conformationally Disordered Phase in a Pseudohexagonal Lattice. The aPAN sample used in this work is conformationally disordered but laterally ordered with pseudohexagonal packing.[1−3,6,10] The local chain direction is aligned with the *c*-axis of the disordered pseudohexagonal lattice of aPAN. In our preceding papers,[1−3] we characterized aPAN as static conformationally disordered (static CONDIS) phase. From our proposed model here, it may be assumed that the nearly

"static" CONDIS phase develops into a "dynamic" CONDIS phase around 110 °C. The distinct "orthorhombic−hexagonal" transition, observed for ultradrawn aPAN fibers,[46] would be related to the more gradual changes in motional rates and amplitudes observed for isotropic powdered aPAN samples in this work.

5. Conclusions

The dynamics of atactic poly(acrylonitrile) have been investigated by one- and two-dimensional solid-state ^{15}N NMR and by dielectric measurements. These detect the motions of the −C≡N side groups, which are rigidly attached to the backbone. A transition in the dynamic behavior is observed at 110 °C. The correlation times follow Arrhenius relations below and above this temperature, but with rather different activation energies of 68 and 180 kJ mol^{-1}, respectively. Thus, this transition should not be termed a glass transition; this is also consistent with the observation that the motion occurs in the disordered pseudohexagonal lattice. The detailed analysis of the NMR spectra shows that aPAN undergoes uniaxially rotational diffusion motion, with amplitudes that are restricted and distributed. Below 110 °C, the standard deviation σ_D of the Gaussian distribution of this motional amplitude increases with temperature, up to ∼30°. The small-angle fluctuations rapidly change to larger-amplitude motions above the transition temperature; σ_D increases from 30 to 100° in the temperature range of 120−140 °C. The increase of motional amplitudes detected by solid-state NMR is in good agreement with the increase of dielectric strength. A previously proposed model of chain motion in aPAN, the five-bond crankshaft mechanism, is not compatible with our experimental findings.

The orientation distribution of the −C≡N groups has been determined from static ^{13}C CSA spectra of uniaxially oriented aPAN fibers with a draw ratio of 15. The average angle and the standard deviation of the Gaussian distribution of the −C≡N groups relative to the chain axis, ($\langle\beta_{CN}\rangle$, σ_β), are found to be between (90°, 17°) and (80°, 14°) at 20 °C. There are strong indications that above 110 °C β_{CN}-averaging motions also occur, which move C≡N bonds through the full range of accessible orientations relative to the chain axis. This means that in the high temperature range the PAN chains do not only rotate around the chains axis but also flex within the channels formed by their six neighboring chains.

All the measurements in this work can be explained by a supramolecular structure consisting essentially of a single morphological phase, although motional and orientational distributions are found to exist. The distributions can be explained by the disorder in the "crystals", which results at least partially from the atactic (configurationally disordered) placement of the side groups.

Acknowledgment. The authors thank Dr. Daisuke Sawai and Professor Tetsuo Kanamoto, Science University of Tokyo, and Mr. Yoshihiro Watanabe, Japan Exlan Co., Ltd. for their helpful advice. K.S.R. thanks the National Science Foundation (DMR 9703916) for funding this work and NSF/MRSEC for support of the NMR facility.

References and Notes

(1) Kaji, H.; Schmidt-Rohr, K. *Macromolecules* **2000**, *33*, 5169.
(2) Kaji, H.; Schmidt-Rohr, K. *Macromolecules* **2001**, *34*, 7368.
(3) Kaji, H.; Schmidt-Rohr, K. *Macromolecules* **2001**, *34*, 7382.
(4) Note that, in the IUPAC definition, torsion angles are classified into four regions; within 30° from 180°, 120°, 60°, and 0°, which correspond to trans (T), anticlinal (A), gauche (G), and cis (C), respectively. The distribution of meso trans−trans dyads of aPAN was too broad, and as a result a peak in the torsion angle distribution extends beyond a single region. In our nomenclature, the designations of T, G, etc. are used for the "average" torsion angle, i.e., the center of a given peak in the torsion angle distribution. Strictly speaking, the 90% trans content does not contain gauche conformations but contains anticlinal conformations. The 10% gauche is strictly detemined. This is described in detail in our preceding papers[1,2] and in Figures 2 and 6 of ref 2.
(5) Bashir, Z. *J. Macromol. Sci., Phys.* **2001**, *B40*, 41.
(6) Bohn, C. R.; Schaefgen, J. R.; Statton, W. O. *J. Polym. Sci.* **1961**, *55*, 531.
(7) Rizzo, P.; Guerra, G.; Auriemma, F. *Macromolecules* **1996**, *29*, 1830.
(8) Minami, S.; Yoshihara, T.; Sato, H. *Kobunshi Kagaku* **1972**, *29*, 114.
(9) Liu, X. D.; Ruland, W. *Macromolecules* **1993**, *26*, 3030.
(10) Rizzo, P.; Auriemma, F.; Guerra, G.; Petraccone, V.; Corradini, P. *Macromolecules* **1996**, *29*, 8852.
(11) Thomsen, T.; Zachmann, H. G.; Korte, S. *Macromolecules* **1992**, *25*, 6934.
(12) According to the studies by Minami et al.[8] and Bashir et al.,[13] the relaxation at 120−160 °C seems to be related to the existence of residual water (or solvent). Therefore, aPAN without solvent shows only one relaxation at 70−110 °C, and a single-phase model looks most appropriate.
(13) Bashir, Z.; Church, S. P.; Waldron, D. *Polymer* **1994**, *35*, 967.
(14) deAzevedo, E. R.; Bonagamba, T. J.; Schmidt-Rohr, K. *J. Magn. Reson.* **2000**, *142*, 86.
(15) Saito, S.; Nakajima, T. *J. Appl. Polym. Sci.* **1953**, *2*, 93.
(16) Hayakawa, R.; Nishi, T.; Arisawa, K.; Wada, Y. *J. Polym. Sci., Part A2* **1967**, *5*, 165.
(17) Okajima, S.; Ikeda, M.; Takeuchi, A. *J. Polym. Sci., Part A1* **1968**, *6*, 1925.
(18) Gupta, A. K.; Chand, N. *J. Polym. Sci., Polym. Phys. Ed.* **1980**, *18*, 1125.
(19) Ishida, Y.; Amano, O.; Takayanagi, M. *Kolloid Z. Z. Polym.* **1960**, *172*, 129.
(20) Natta, G.; Mazzanti, G.; Corradini, P. *Atti Accad. Naz. Lincei, Cl. Sci. Fis. Mater. Nat., Rend.* **1958**, *25*, 3.
(21) Lindenmeyer, P. H.; Hosemann, R. *J. Appl. Phys.* **1963**, *34*, 42.
(22) See references in ref 1.
(23) Kaplan, M. L.; Bovey, F. A.; Chang, H. V. *Anal. Chem.* **1975**, *47*, 1703.
(24) Tsuji, H.; Horii, F.; Nakagawa, M.; Ikada, Y.; Odani, H.; Kitamaru, R. *Macromolecules* **1992**, *25*, 4114.
(25) Bielecki, A.; Burum, D. P. *J. Magn. Reson. A* **1995**, *116*, 215.
(26) Takahashi, T.; Kawashima, H.; Sugisawa, H.; Baba, T. *Solid State Nucl. Magn. Reson.* **1999**, *15*, 119.
(27) Mathias, L. J.; Colletti, R. F. *Macromolecules* **1991**, *24*, 5515.
(28) Schaefer, D.; Spiess, H. W. *J. Chem. Phys.* **1992**, *97*, 7944.
(29) Becker, H. J. Diploma work, Dortmund, 1975.
(30) Spiess, H. W.; Sillescu, H. *J. Magn. Reson.* **1981**, *42*, 381.
(31) Tonelli, A. E. *NMR Spectroscopy and Polymer Microstructure: The Conformational Connection*; VCH Publishers: New York, 1989.
(32) The misalignment of the oriented aPAN fibers, σ_{mis} (<5°), is mostly negligible, since the real standard deviation of distribution, σ_{real}, is obtained from the relation $\sigma_\beta^2 = \sigma_{mis}^2 + \sigma_{real}^2$. For $\sigma_\beta = 17°$ and 14° and $\sigma_{mis} < 5°$, σ_{real} is calculated to be >16.2° and >13.1°, respectively.
(33) Even without distribution of CN side-group directions, the CSA pattern of Figure 7f is not symmetric, although each of the three subpatterns, shown by dotted lines, is symmetric. This is because the splitting for the downfield peaks is 17 ppm while that for upfield peaks is 34 ppm.
(34) Bashir, Z.; Tipping, A. R.; Church, S. P. *Polym. Int.* **1994**, *33*, 9.
(35) Torchia, D. A.; Szabo, A. *J. Magn. Reson.* **1982**, *49*, 107.
(36) Wefing, S. Ph.D. Thesis, University Mainz, 1988.
(37) Cotten, G. R.; Schneider, W. C. *Kolloid Z. Z. Polym.* **1963**, *192*, 16.
(38) Ishida, Y.; Matsuo, M.; Ueno, Y.; Takayanagi, M. *Kolloid Z. Z. Polym.* **1964**, *199*, 67.
(39) The angle depends on the opening angle, β_{CN}, between the rotation axis and the CN direction. In the case of three-site crankshaft motion, the angle before and after the jump, ϕ_j,

is calculated as $\cos \phi_j = \cos 120° \times \sin^2 \beta_{CN} + \cos^2 \beta_{CN}$. The angle $\phi_j = 112°$ for $\beta_{CN} = 73.4°$.

(40) Hu, W. G.; Boeffel, C.; Schmidt-Rohr, K. *Macromolecules* **1999**, *32*, 1611. Hu, W. G.; Boeffel, C.; Schmidt-Rohr, K. *Macromolecules* **1999**, *32*, 1714.

(41) Mowry, S. W.; Rutledge, G. C. *Macromolecules* **2002**, *35*, 4539.

(42) Mansfield, M. L.; Boyd, R. H. *J. Polym. Sci., Polym. Phys. Ed.* **1978**, *16*, 1227.

(43) Boyd, R. H. *Polymer* **1985**, *26*, 1123.

(44) The underlying principle of symmetrization of the ^{2}H spectrum due to the presence of two transitions is shown in various introductory NMR texts. The direct comparison of a CN CSA pattern and a C$-^2$H quadrupolar pattern is given in Figure 2.4 in: Schmidt-Rohr, K.; Spiess, H. W. *Multidimensional Solid-State NMR and Polymers*; Academic Press: London, 1994.

(45) $\kappa_1/\kappa_2 = \exp(\Delta E_a/R(1/T_1 - 1/T_2))$. The value of $1000/(1/T_1 - 1/T_2) = 0.1205$ K^{-1}, when $\kappa_1/\kappa_2 = 13.6$, $\Delta E_a = 180$ kJ mol^{-1}, and $R = 8.31$ J mol^{-1} K^{-1}.

(46) Sawai, D.; Kanamoto, T.; Porter, R. S. *Macromolecules* **1998**, *31*, 2010.

MA0341420